Supporting Information

Discovery of Irreversible p97 Inhibitors

*Rui Ding, Ting Zhang, Daniel J. Wilson, Jiashu Xie, Jessica Williams, Yue Xu, Yihong Ye, and Liqiang Chen**

Table of contents:

- **Table S1.** DTT reactivity of selected compounds: S2
- **Table S2.** List of p97 peptides that were covalently modified by compound **20**: S4
- **Table S3.** K_i^{app} values at increasing ATP concentrations: S5
- **Table S4.** Active site (within D2 domain) Glide XP docking scores: S7
- **Table S5.** CovDock docking scores: S8
- **Figure S1.** Degradation of ΔSS TCRα-YFP in the presence of proteasome or p97 inhibitors: S9
- **Figure S2.** Examples of tandem mass spectra of peptides that were covalently modified by compound **20** at (**A**) Cys105, (**B**) Cys522, and (**C**) Cys535: S10
- **Figure S3.** Three cysteine residues (Cys105, 522, and 535) in human p97 (PDB 5FTK, subunit E) as potential targets of compound **20**: S11
- **Figure S4.** A 2D representation of potential interactions between compound **4b** and p97: S12
- **Figure S5.** Proposed binding mode and interactions of compound **4b** docked into the cryo-EM structure of human p97 (PDB 5FTK) using subunit E as a template: S13
- **Figure S6.** A 2D representation of potential interactions between compound **19** and p97: S14
- **Figure S7.** A 2D representation of potential interactions between compound **22** and p97: S15
- **Figure S8.** Proposed binding modes of **S1** (green), **S2** (cyan) and **S3** (magenta) docked (XP mode) into the cryo-EM structure of human p97 (PDB 5FTK) at the active site of the D2 domain: S16
- **Figure S9.** Proposed binding modes of **S1** (green), **S2** (cyan) and **S3** (magenta) covalently docked into the cryo-EM structure of human p97 (PDB 5FTK) at the active site of the D2 domain: S17
- **Figure S10.** Proposed binding modes and interactions of compounds **11** (magenta) and **15** (green) docked into the cryo-EM structure of human p97 (PDB 5FTK) at the active site of the D2 domain: S18

Table S1. DTT reactivity of selected compounds.

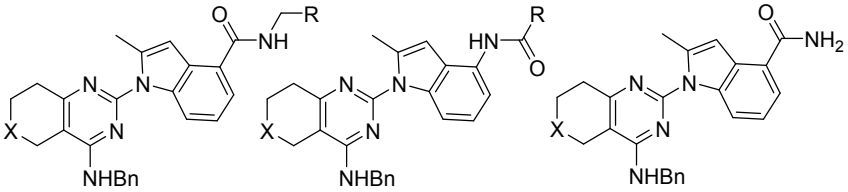

Cmpd	Core	X	R	GSH reactivity $t_{1/2}$ (h)	GSH adduct	DTT reactivity $t_{1/2}$ (h)
11	I	CH_2	C≡CH	> 24	no	--
12	I	CH_2	C≡N	> 24	no	--
13	I	CH_2	$CH_2C{\equiv}CH$	--	--	--
14	I	CH_2	$CH_2C{\equiv}N$	--	--	--
15	I	CH_2	C≡CMe	> 24	no	--
16	I	CH_2	Et	--	--	--
17	I	O	C≡CH	> 24	no	--
18	I	O	C≡CMe	> 24	no	--
19	II	CH_2	C≡CH	0.21	yes	0.23
20	II	CH_2	C≡CMe	16.4	yes	> 24
21	II	CH_2	C≡CEt	13.5	yes	> 24
22	II	CH_2	C≡C^{n}Pr	21.6	yes	> 24
23	II	CH_2	$CH{=}CH_2$	5.08	yes	7.48
24	II	CH_2	Et	--	--	--
25	II	O	C≡CH	0.21	yes	0.27
26	II	O	C≡CMe	16.2	yes	> 24
27	II	O	$CH{=}CH_2$	4.31	yes	6.26
4a	III	CH_2	--	--	--	--
4b	III	O	--	--	--	> 24

DTT Reactivity Assay. To assess reactivity with DTT, the test compounds (1 μM) were incubated at 37 °C with 1 mM DTT and a stable internal standard in the reaction buffer (50 mM Tris HCl pH 8.0, 150 mM KCl, 1 mM $MgCl_2$, 15% glycerol) in a total volume of 1 mL. The reactions were initiated upon addition of DTT, and the samples were analyzed by directly injected the mixture into LC-MS/MS immediately after the DTT addition and then at predetermined intervals within a 12 h period. Control reactions were run in the absence of DTT. The disappearance of parent compounds were monitored as % remaining relative to time zero, and the data were fitted to first-order kinetics by plotting the natural log of % remaining as a function of time. The pseudo-first-order rate constant (k), which is the negative slope of the linear fitting, was used to calculate the reaction half-life ($t_{1/2} = 0.693/k$).

Table S2. List of p97 peptides that were covalently modified by compound 20.

ScanF	z	PPM	XCorr	ΔCorr	# Ions	Reference	Sequest Peptide	ModScore Peptide_A	Site 1 PositionA	Site 1 ScoreA	ModScore Peptide_B	Site 1 PositionB	Site 1 ScoreB
29123	3	1.01	2.235	0.604	17/52	sp|Q01853|TERA_MOUSE	K.AIANEC#QANFISIK.G	K.AIANEC#QANFISIK.G	535	22.5	K.AIANEC#QANFISIK.G	535	28.7
29139	3	1.09	2.279	0.469	19/52	sp|Q01853|TERA_MOUSE	K.AIANEC#QANFISIK.G	K.A#IANECQANFISIK.G	530	0.0	K.A#IANECQANFISIK.G	530	0.0
29344	3	1.26	2.059	0.53	18/52	sp|Q01853|TERA_MOUSE	K.AIANEC#QANFISIK.G	K.AIANEC#QANFISIK.G	535	6.3	K.AIANEC#QANFISIK.G	535	2.4
29732	3	2.33	1.656	0.457	15/52	sp|Q01853|TERA_MOUSE	K.AIANEC#QANFISIK.G	K.AIANEC#QANFISIK.G	535	10.8	K.AIANEC#QANFISIK.G	535	13.0
29995	3	2	1.853	0.545	16/52	sp|Q01853|TERA_MOUSE	K.AIANEC#QANFISIK.G	K.AIANEC#QANFISIK.G	535	6.3	K.A#IANECQANFISIK.G	530	0.0
33106	3	1.49	2.125	0.687	20/44	sp|Q01853|TERA_MOUSE	K.GVLFYGPPGC#GK.T	K.GVLFYGPPGC#GK.T	522	42.9	K.GVLFYGPPGC#GK.T	522	42.1
33190	2	2.32	1.927	0.743	22-Oct	sp|Q01853|TERA_MOUSE	K.GVLFYGPPGC#GK.T	K.GVLFYGPPGC#GK.T	522	33.7	K.GVLFYGPPGC#GK.T	522	47.9
33221	3	1.45	1.649	0.583	14/44	sp|Q01853|TERA_MOUSE	K.GVLFYGPPGC#GK.T	K.GVLFYGPPGC#GK.T	522	19.0	K.GVLFYGPPGC#GK.T	522	31.9
33401	2	2.49	1.871	0.678	22-Aug	sp|Q01853|TERA_MOUSE	K.GVLFYGPPGC#GK.T	K.GVLFYGPPGC#GK.T	522	23.6	K.GVLFYGPPGC#GK.T	522	23.1
33451	3	1.45	1.78	0.727	13/44	sp|Q01853|TERA_MOUSE	K.GVLFYGPPGC#GK.T	K.GVLFYGPPGC#GK.T	522	26.1	K.GVLFYGPPGC#GK.T	522	22.7
32447	3	1.89	3.111	0.561	19/52	sp|Q01853|TERA_MOUSE	R.LGDVISIQPC#PDVK.Y	R.LGDVISIQPC#PDVK.Y	105	46.1	R.LGDVISIQPC#PDVK.Y	105	48.3
32554	3	1.75	3.011	0.482	21/52	sp|Q01853|TERA_MOUSE	R.LGDVISIQPC#PDVK.Y	R.LGDVISIQPC#PDVK.Y	105	37.5	R.LGDVISIQPC#PDVK.Y	105	28.7
32669	3	1.62	3.062	0.545	19/52	sp|Q01853|TERA_MOUSE	R.LGDVISIQPC#PDVK.Y	R.LGDVISIQPC#PDVK.Y	105	37.5	R.LGDVISIQPC#PDVK.Y	105	38.1
32784	3	1.56	3.49	0.725	19/52	sp|Q01853|TERA_MOUSE	R.LGDVISIQPC#PDVK.Y	R.LGDVISIQPC#PDVK.Y	105	37.5	R.LGDVISIQPC#PDVK.Y	105	48.3
32899	3	1.5	3.129	0.748	18/52	sp|Q01853|TERA_MOUSE	R.LGDVISIQPC#PDVK.Y	R.LGDVISIQPC#PDVK.Y	105	46.1	R.LGDVISIQPC#PDVK.Y	105	48.3
33014	3	1.4	3.03	0.586	21/52	sp|Q01853|TERA_MOUSE	R.LGDVISIQPC#PDVK.Y	R.LGDVISIQPC#PDVK.Y	105	55.4	R.LGDVISIQPC#PDVK.Y	105	59.2
33129	3	1.33	2.808	0.58	19/52	sp|Q01853|TERA_MOUSE	R.LGDVISIQPC#PDVK.Y	R.LGDVISIQPC#PDVK.Y	105	29.7	R.LGDVISIQPC#PDVK.Y	105	6.9
33245	3	1.39	2.583	0.438	19/52	sp|Q01853|TERA_MOUSE	R.LGDVISIQPC#PDVK.Y	R.LGDVISIQPC#PDVK.Y	105	37.5	R.LGDVISIQPC#PDVK.Y	105	48.3
33360	3	1.58	3.417	0.583	19/52	sp|Q01853|TERA_MOUSE	R.LGDVISIQPC#PDVK.Y	R.LGDVISIQPC#PDVK.Y	105	55.4	R.LGDVISIQPC#PDVK.Y	105	48.3
33481	3	2.04	3.273	0.437	18/52	sp|Q01853|TERA_MOUSE	R.LGDVISIQPC#PDVK.Y	R.LGDVISIQPC#PDVK.Y	105	37.5	R.LGDVISIQPC#PDVK.Y	105	28.7
33621	3	1.82	2.801	0.413	20/52	sp|Q01853|TERA_MOUSE	R.LGDVISIQPC#PDVK.Y	R.LGDVISIQPC#PDVK.Y	105	37.5	R.LGDVISIQPC#PDVK.Y	105	38.1
33725	3	1.58	2.899	0.423	19/52	sp|Q01853|TERA_MOUSE	R.LGDVISIQPC#PDVK.Y	R.LGDVISIQPC#PDVK.Y	105	16.2	R.LGDVISIQPC#PDVK.Y	105	20.3
33737	3	1.45	2.684	0.478	19/52	sp|Q01853|TERA_MOUSE	R.LGDVISIQPC#PDVK.Y	R.LGDVISIQPC#PDVK.Y	105	55.4	R.LGDVISIQPC#PDVK.Y	105	48.3
33835	3	1.34	2.961	0.748	17/52	sp|Q01853|TERA_MOUSE	R.LGDVISIQPC#PDVK.Y	R.LGDVISIQPC#PDVK.Y	105	46.1	R.LGDVISIQPC#PDVK.Y	105	38.1
33940	3	1.49	4.046	0.665	21/52	sp|Q01853|TERA_MOUSE	R.LGDVISIQPC#PDVK.Y	R.LGDVISIQPC#PDVK.Y	105	75.7	R.LGDVISIQPC#PDVK.Y	105	70.9
34060	3	1.8	3.232	0.501	18/52	sp|Q01853|TERA_MOUSE	R.LGDVISIQPC#PDVK.Y	R.LGDVISIQPC#PDVK.Y	105	37.5	R.LGDVISIQPC#PDVK.Y	105	38.1
34154	3	1.94	2.804	0.645	17/52	sp|Q01853|TERA_MOUSE	R.LGDVISIQPC#PDVK.Y	R.LGDVISIQPC#PDVK.Y	105	46.1	R.LGDVISIQPC#PDVK.Y	105	48.3
34332	3	1.71	2.899	0.405	19/52	sp|Q01853|TERA_MOUSE	R.LGDVISIQPC#PDVK.Y	R.LGDVISIQPC#PDVK.Y	105	46.1	R.LGDVISIQPC#PDVK.Y	105	59.2
34496	3	1.79	2.808	0.624	18/52	sp|Q01853|TERA_MOUSE	R.LGDVISIQPC#PDVK.Y	R.LGDVISIQPC#PDVK.Y	105	22.5	R.LGDVISIQPC#PDVK.Y	105	38.1
34610	3	2	2.148	0.463	16/52	sp|Q01853|TERA_MOUSE	R.LGDVISIQPC#PDVK.Y	R.LGDVISIQPC#PDVK.Y	105	37.5	R.LGDVISIQPC#PDVK.Y	105	20.3
34752	3	2.13	2.343	0.397	17/52	sp|Q01853|TERA_MOUSE	R.LGDVISIQPC#PDVK.Y	R.LGDVISIQPC#PDVK.Y	105	37.5	R.LGDVISIQPC#PDVK.Y	105	48.3
35367	3	1.97	2.637	0.383	19/52	sp|Q01853|TERA_MOUSE	R.LGDVISIQPC#PDVK.Y	R.LGDVISIQPC#PDVK.Y	105	37.5	R.LGDVISIQPC#PDVK.Y	105	48.3

Table S3. K_i^{app} values at increasing ATP concentrations.

ATP (mM)	Compound **20** K_i^{app} (nM)
0.312	9.93 ± 1.45
0.625	15.3 ± 1.7
1.25	22.4 ± 2.1
2.50	23.8 ± 2.2
5.00	18.0 ± 1.9

Determination of K_i^{app} values at increasing ATP concentrations. In order to more precisely measure enzyme activity and inhibition the p97 biochemical assay was modified from the continuous format to a two-step endpoint assay. The initial p97 reaction was carried out in 96 well non-binding surface black microplates at the final volume of 100 µL. Each reaction contained 15% glycerol, 150 mM KCl, 50 mM Tris HCL pH 8.0, 1 mM $MgCl_2$, 1 mM DTT, 0.0058 µg/µL p97 (~60 nM) and 0–11.1 µM inhibitor in duplicate. Reactions were incubated with inhibitor for 10 min and then initiated by the addition of ATP (5 µL) for a final concentration of 0.3125, 0.625, 1.25, 2.5 or 5 mM. Reactions were mixed and incubated at 37 °C for 2 h after which 78 µL was transferred to a UV clear half area 96 well plate containing 22 µL of development solution (2 U/mL PNP, 200 mM MesG final concentration). The plates were incubated for an additional 10 min at room temperature and read at 360 nm on an i3 multi-mode microplate reader. The velocities were fit to the Morrison equation using Prism 5 (GraphPad) to generate K_i^{app} values.

Table S4. Active site (within D2 domain) Glide XP docking scores.

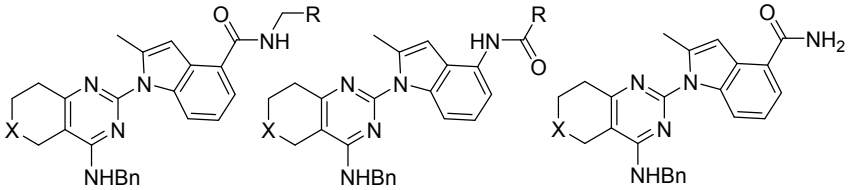

I **II** **III**

Cmpd	Core	X	R	K_i^{app} (nM)	XP docking score
11	I	CH_2	C≡CH	30.6 ± 3.8	–5.240
12	I	CH_2	C≡N	28.1 ± 3.6	–5.484
13	I	CH_2	CH_2C≡CH	24.5 ± 3.3	–5.885
14	I	CH_2	CH_2C≡N	24.1 ± 3.3	–5.389
15	I	CH_2	C≡CMe	37.3 ± 4.3	–2.608
16	I	CH_2	Et	40.8 ± 4.5	–6.121
17	I	O	C≡CH	18.6 ± 2.9	–3.808
18	I	O	C≡CMe	42.4 ± 4.6	–4.846
19	II	CH_2	C≡CH	37.9 ± 4.3	–4.967
20	II	CH_2	C≡CMe	33.2 ± 4.0	–6.049
21	II	CH_2	C≡CEt	43.0 ± 4.7	–6.283
22	II	CH_2	C≡C^{n}Pr	26.9 ± 3.5	–6.741
23	II	CH_2	CH=CH_2	31.4 ± 3.8	–4.980
24	II	CH_2	Et	20.8 ± 3.1	–5.083
25	II	O	C≡CH	32.8 ± 3.9	–4.486
26	II	O	C≡CMe	32.3 ± 3.9	–4.837
27	II	O	CH=CH_2	26.6 ± 3.5	–5.555
4a	III	CH_2	--	28.6 ± 3.6	–5.183
4b	III	O	--	26.1 ± 7.0	5.337

Table S5. CovDock docking scores.

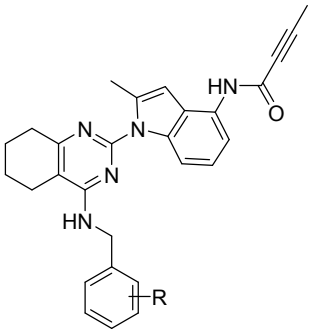

Cmpd	R	Active site (Cys522) XP	Cys522 CovDock	Cys535 XP	Cys535 CovDock	Cys105 XP	Cys105 CovDock
20	H	–6.049	–5.755	–6.132	–4.054	–2.585	–3.130
S1	2-Me	6.214	6.827				
S2	3-Me	6.570	7.283				
S3	4-Me	6.418	5.318				

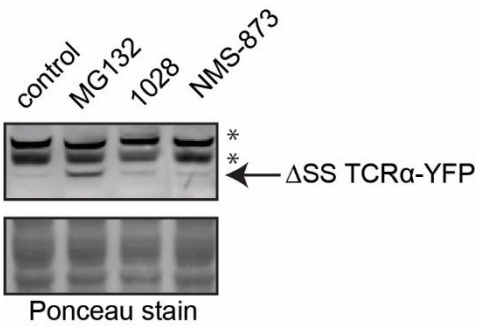

Figure S1. Degradation of ΔSS TCRα-YFP in the presence of proteasome or p97 inhibitors (1028 = compound **20**). 0.8 M 293T cells stably expressing YFP delSS TCRa were seeded in 6 well plate on day 1 and incubated overnight. 10 μM MG132 or 2 μM p97 inhibitors was added to the cell on day 2 and incubated overnight. Cells were harvested on day 3 and lysed in NP40 lysis buffer. Cell extracts were analyzed by WB.

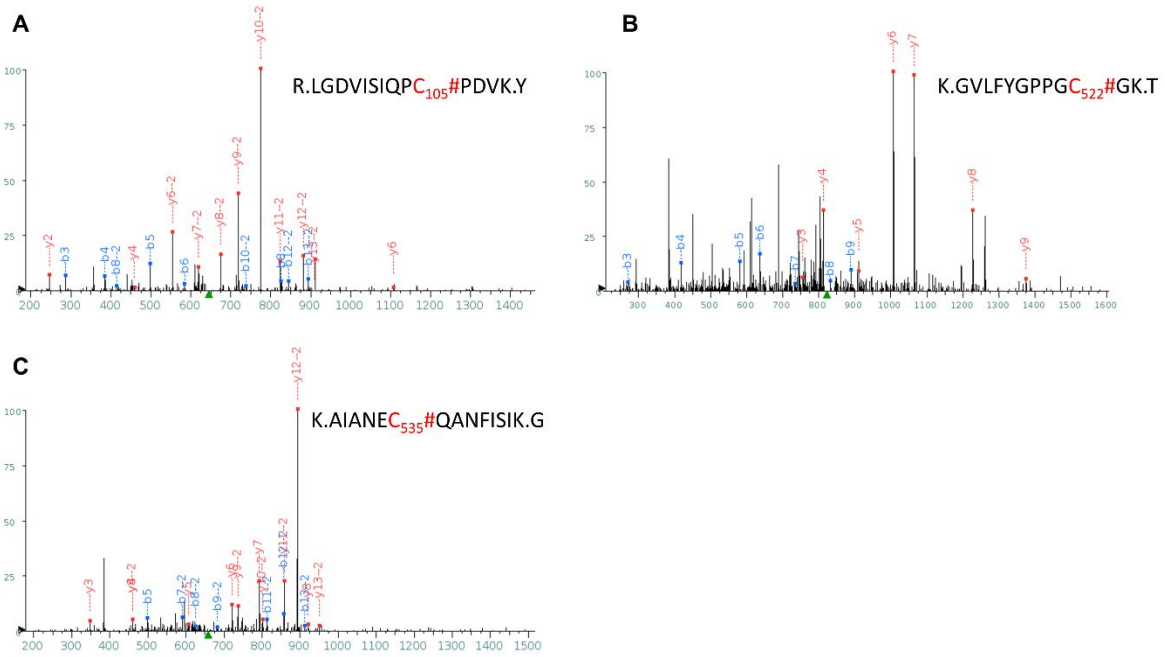

Figure S2. Examples of tandem mass spectra of peptides that were covalently modified by compound **20** at (**A**) Cys105, (**B**) Cys522, and (**C**) Cys535.

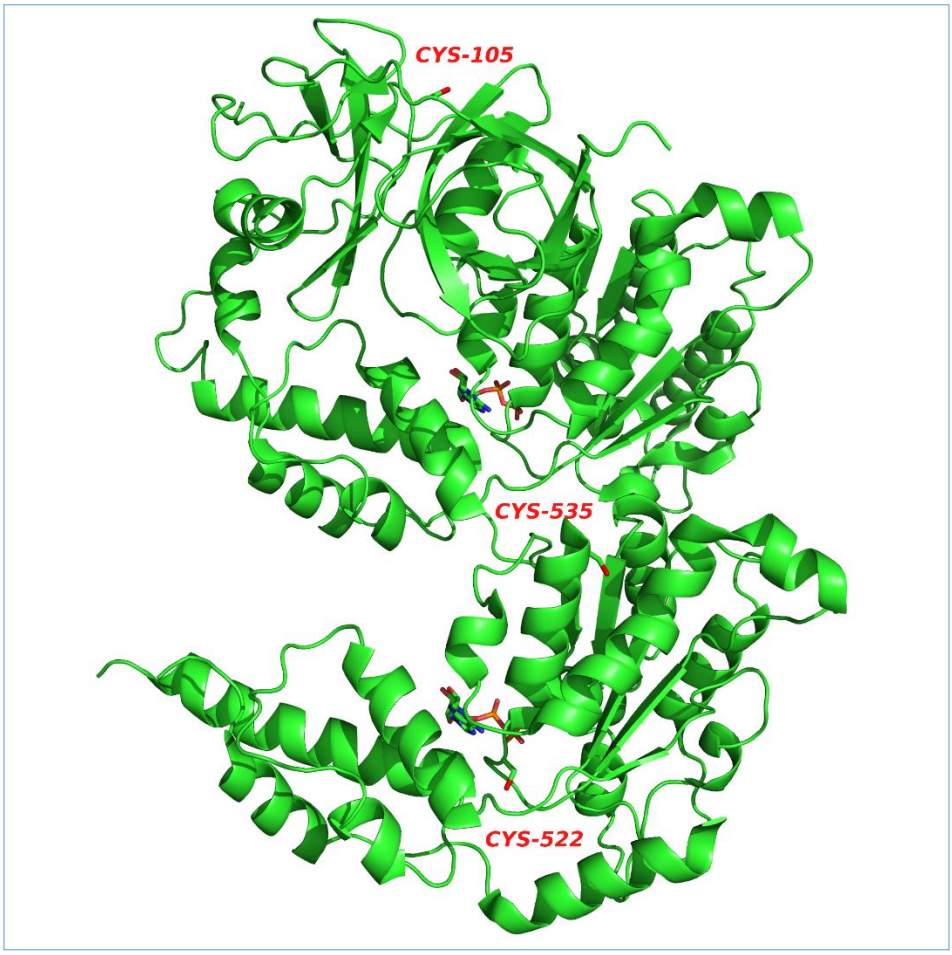

Figure S3. Three cysteine residues (Cys105, 522, and 535) in human p97 (PDB 5FTK, subunit E) as potential targets of compound **20**.

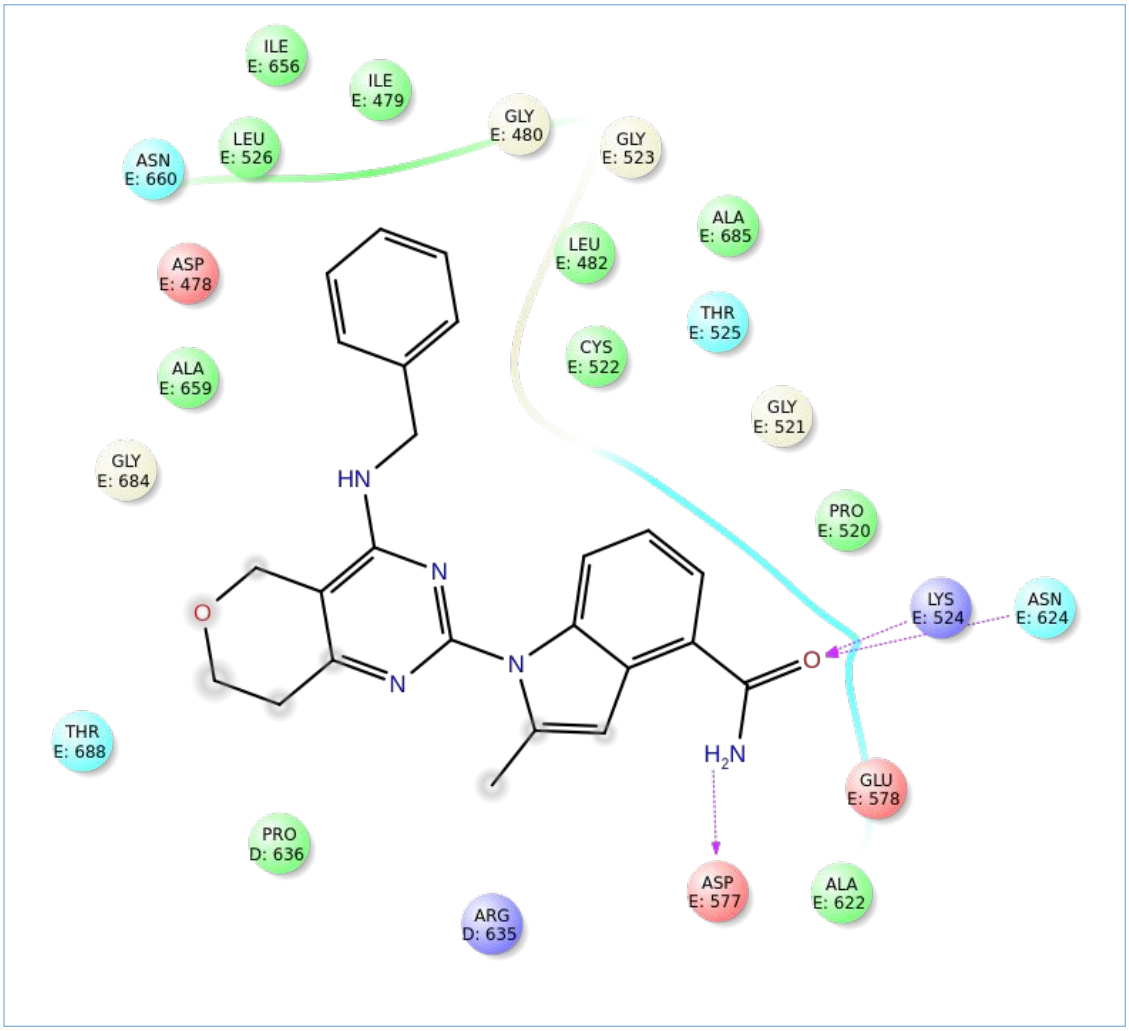

Figure S4. A 2D representation of potential interactions between compound **4b** and p97.

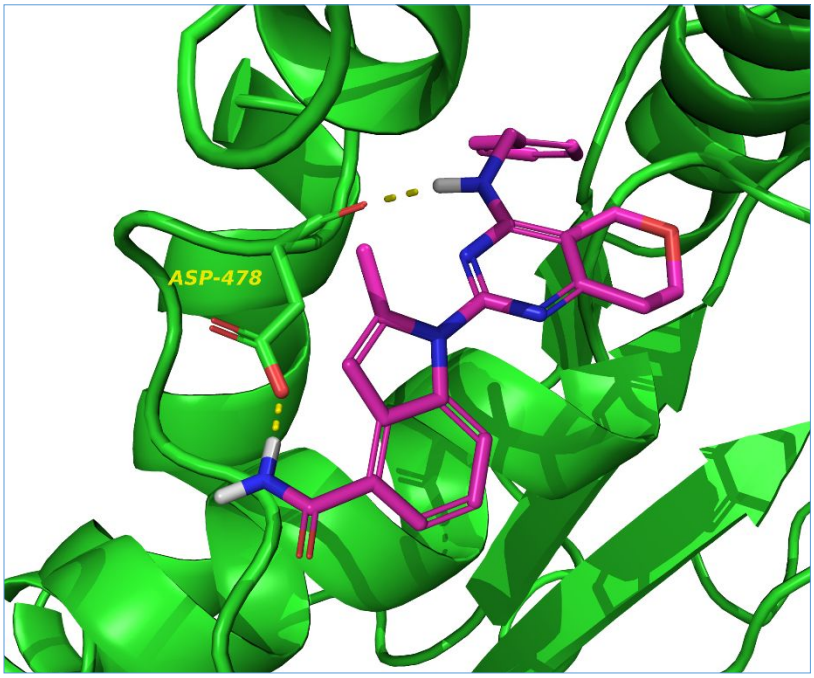

Figure S5. Proposed binding mode and interactions of compound **4b** docked into the cryo-EM structure of human p97 (PDB 5FTK) using subunit E as a template.

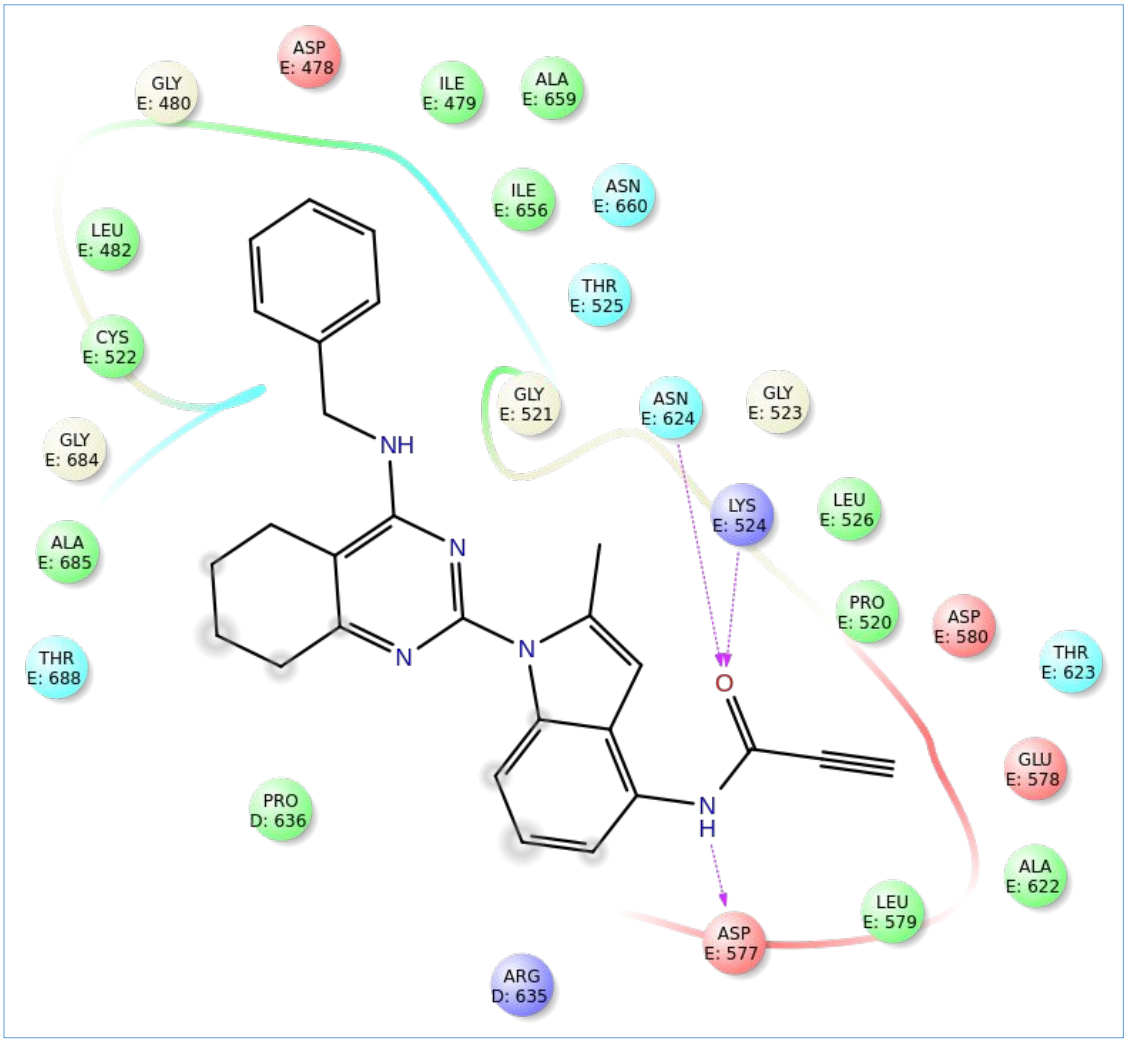

Figure S6. A 2D representation of potential interactions between compound **19** and p97.

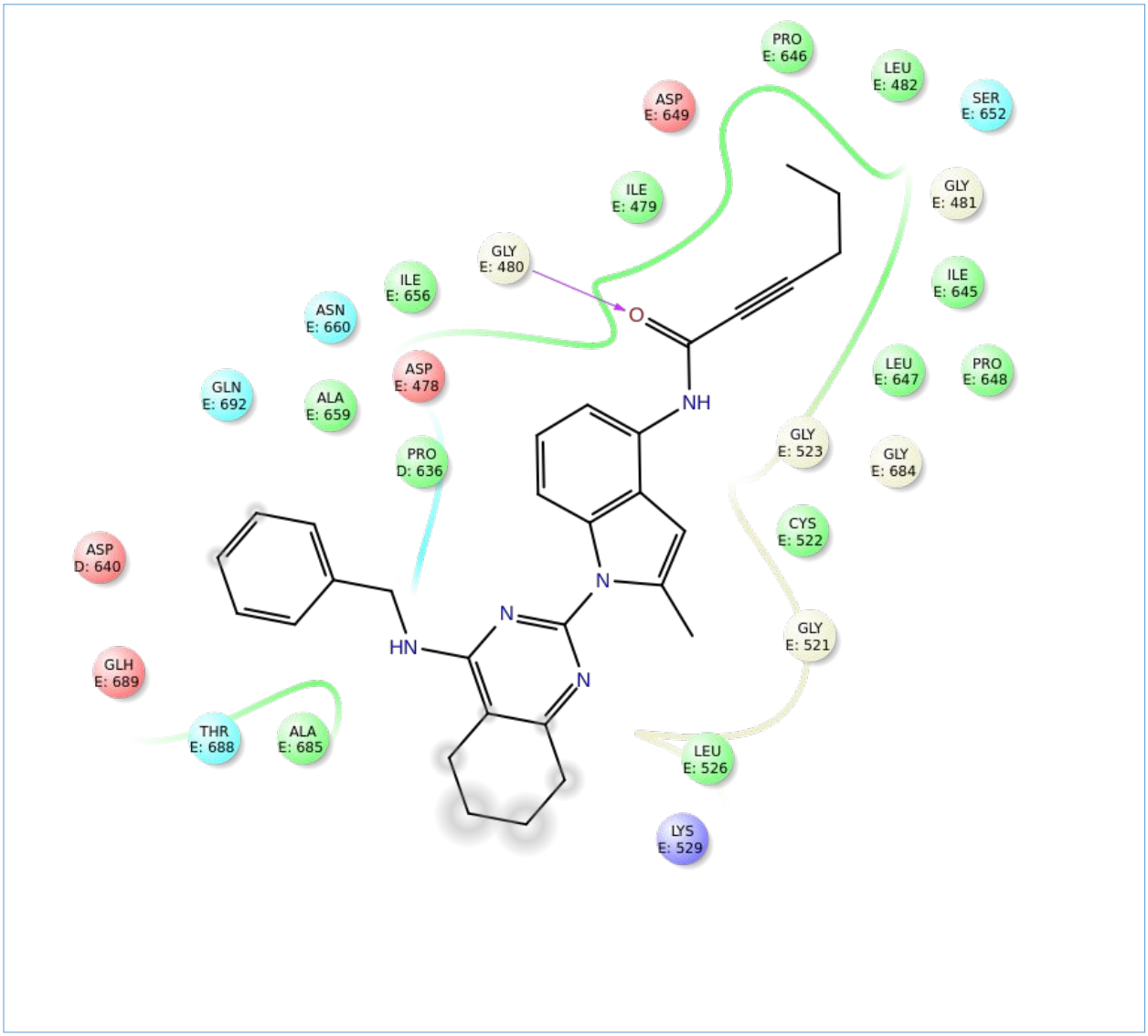

Figure S7. A 2D representation of potential interactions between compound **22** and p97.

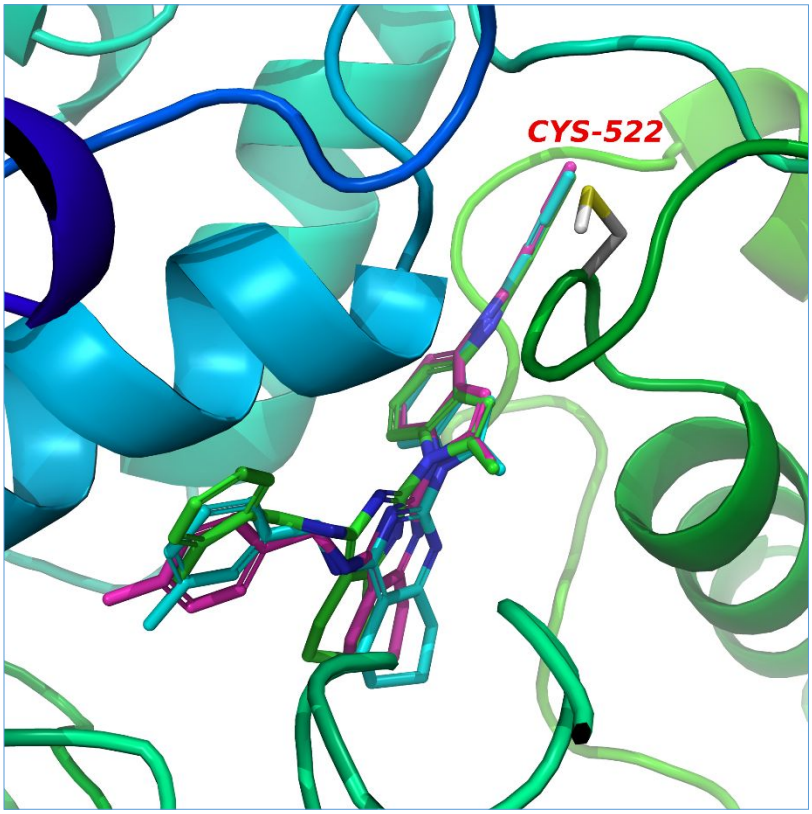

Figure S8. Proposed binding modes of **S1** (green), **S2** (cyan) and **S3** (magenta) docked (XP mode) into the cryo-EM structure of human p97 (PDB 5FTK) at the active site of the D2 domain.

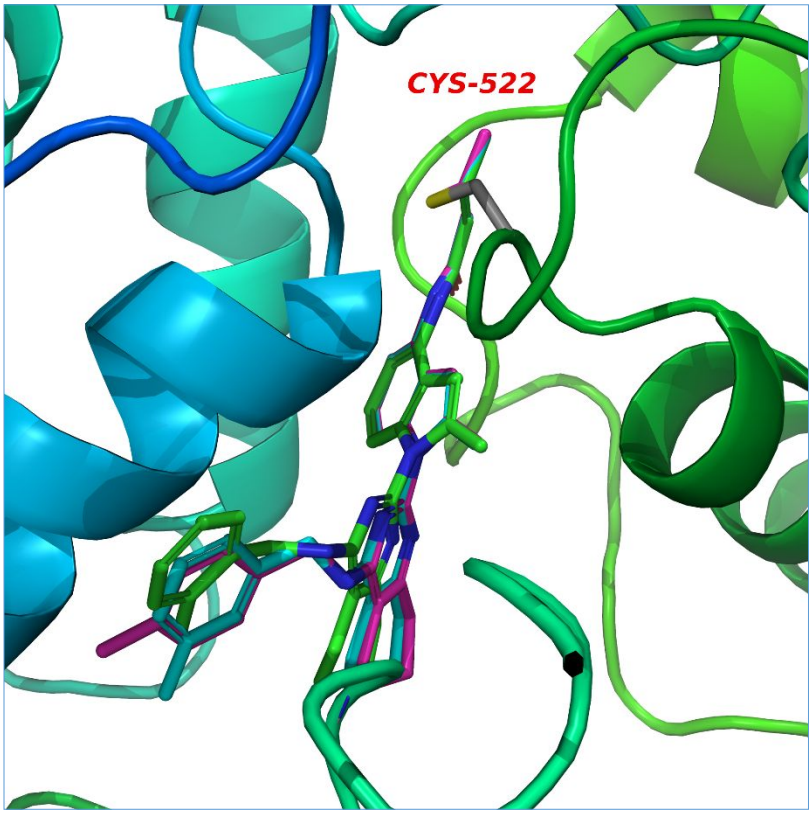

Figure S9. Proposed binding modes of **S1** (green), **S2** (cyan) and **S3** (magenta) covalently docked into the cryo-EM structure of human p97 (PDB 5FTK) at the active site of the D2 domain. Unlike compound **20**, there was no significant change of inhibitor orientation upon covalent bond formation.

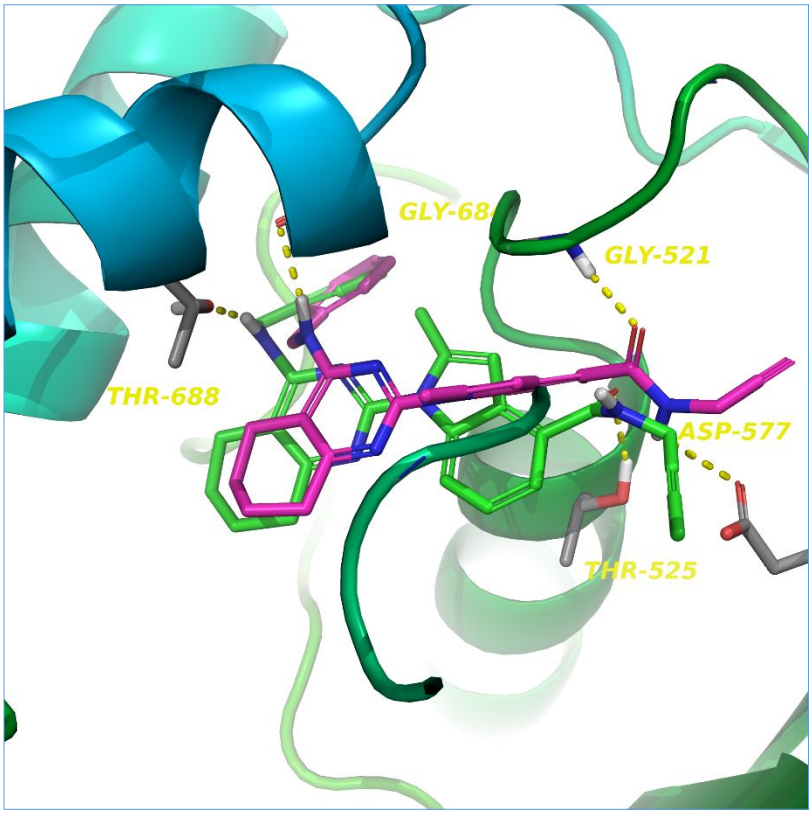

Figure S10. Proposed binding modes and interactions of compounds **11** (magenta) and **15** (green) docked into the cryo-EM structure of human p97 (PDB 5FTK) at the active site of the D2 domain.